NASA TECHNICAL NOTE



NASA TN D-6595

# PREDICTION OF LOCAL AND INTEGRATED HEAT TRANSFER IN NOZZLES USING AN INTEGRAL TURBULENT BOUNDARY LAYER METHOD

*by Donald R. Boldman, James F. Schmidt, and Robert C. Ehlers*

*Lewis Research Center*
*Cleveland, Ohio 44135*

NATIONAL AERONAUTICS AND SPACE ADMINISTRATION • WASHINGTON, D. C. • MARCH 1972

| 1. Report No. | 2. Government Accession No. | 3. Recipient's Catalog No. |
|---|---|---|
| NASA TN D-6595 | | |

| 4. Title and Subtitle | 5. Report Date |
|---|---|
| PREDICTION OF LOCAL AND INTEGRATED HEAT TRANSFER IN NOZZLES USING AN INTEGRAL TURBULENT BOUNDARY LAYER METHOD | March 1972 |
| | 6. Performing Organization Code |
| 7. Author(s) | 8. Performing Organization Report No. |
| Donald R. Boldman, James F. Schmidt, and Robert C. Ehlers | E-6669 |
| | 10. Work Unit No. 132-15 |
| 9. Performing Organization Name and Address | 11. Contract or Grant No. |
| Lewis Research Center<br>National Aeronautics and Space Administration<br>Cleveland, Ohio 44135 | |
| | 13. Type of Report and Period Covered |
| 12. Sponsoring Agency Name and Address | Technical Note |
| National Aeronautics and Space Administration<br>Washington, D.C. 20546 | 14. Sponsoring Agency Code |

15. Supplementary Notes

16. Abstract

An empirical modification of an existing integral energy turbulent boundary layer method is proposed in order to improve the estimates of local heat transfer in converging-diverging nozzles and consequently, provide better assessments of the total or integrated heat transfer. The method involves the use of a modified momentum-heat analogy which includes an acceleration term comprising the nozzle geometry and free stream velocity. The original and modified theories are applied to heat transfer data from previous studies which used heated air in $30^{\circ}$-$15^{\circ}$, $45^{\circ}$-$15^{\circ}$, and $60^{\circ}$-$15^{\circ}$ water-cooled nozzles.

| 17. Key Words (Suggested by Author(s)) | 18. Distribution Statement |
|---|---|
| Boundary layer<br>Heat transfer<br>Nozzles | Unclassified - unlimited |

| 19. Security Classif. (of this report) | 20. Security Classif. (of this page) | 21. No. of Pages | 22. Price* |
|---|---|---|---|
| Unclassified | Unclassified | 29 | $3.00 |

* For sale by the National Technical Information Service, Springfield, Virginia 22151

# PREDICTION OF LOCAL AND INTEGRATED HEAT TRANSFER IN NOZZLES USING AN INTEGRAL TURBULENT BOUNDARY LAYER METHOD

by Donald R. Boldman, James F. Schmidt, and Robert C. Ehlers

Lewis Research Center

## SUMMARY

An integral turbulent boundary layer theory was applied to heat transfer data from previous heated air studies in $30^{\circ}$-$15^{\circ}$, $45^{\circ}$-$15^{\circ}$, and $60^{\circ}$-$15^{\circ}$ water-cooled nozzles. The data for the $30^{\circ}$-$15^{\circ}$ and $60^{\circ}$-$15^{\circ}$ nozzles were obtained at a maximum stagnation pressure and temperature of 207 N/cm$^2$ absolute and 539 K, respectively. The $45^{\circ}$-$15^{\circ}$ nozzle data was obtained from a different facility which provided a stagnation pressure and temperature of 172 N/cm$^2$, absolute and 811 K, respectively.

The results of this study indicated that a general improvement in estimates of local heat transfer and integrated or total heat transfer in the nozzle could be obtained by altering the original theory (energy method). Specifically, the original auxiliary equation in the energy method was modified to include an acceleration term involving the nozzle geometry and free stream velocity.

## INTRODUCTION

The convective heat transfer associated with a turbulent boundary layer in highly accelerated flows has been the subject of numerous studies in the last decade. The previously reported work of references 1 to 4 disclosed that (1) changes in upstream boundary layer momentum history (resulting from different length uncooled inlets) were not important in establishing the level of heat transfer in a nozzle, and (2) the energy thickness Reynolds number in the integral boundary layer analysis of reference 5 provided a good criterion for estimating throat heat transfer. However, estimates of the heat transfer in the nozzle entrance region, based on the latter integral boundary layer theory as well as the differential (similar-solution) analysis of reference 6, were often much lower than the measured values. In current designs of extremely high performance nozzles, improved predictions of local heat flux in regions other than the nozzle throat are

required in order to more accurately determine the overall nozzle performance. The performance can depend, in part, on an assessment of the integrated or total heat loss in the nozzle.

In the present study an empirical modification of the integral boundary layer theory of reference 5 is presented in order to provide a better description of the nozzle heat transfer distribution. The local values of heat flux will be integrated along the nozzle to indicate the differences in predicted total heat flux resulting from the modified theory. The boundary layer analysis is applied to the data of previous nozzle heat transfer studies conducted in a heated air facility at the NASA Lewis Research Center (refs. 1 and 3) and also to data from the heated-air studies of nozzle heat transfer by Back, Massier, and Cuffel (ref. 2).

## SYMBOLS

| | |
|---|---|
| A | nozzle surface area |
| $C_f$ | skin friction coefficient |
| $C_p$ | specific heat at constant pressure |
| D | local diameter |
| M | Mach number |
| N | interaction exponent |
| P | pressure |
| Pr | Prandtl number |
| q | heat transfer rate |
| Q | integrated heat flux, eq. (7) |
| $Q^*$ | integrated heat flux from nozzle entrance to throat |
| $Q_T$ | total heat flux in nozzle |
| R | local radius |
| Re | Reynolds number |
| $\mathcal{R}$ | recovery factor |
| S | distance along wall starting from cone entrance |
| St | Stanton number |
| T | temperature |
| u | velocity |

x axial distance from throat

y distance from wall

z axial distance from nozzle entrance

$\delta$ velocity boundary layer thickness

$\delta^*$ displacement thickness

$\Delta$ thermal boundary layer thickness

$\theta$ momentum thickness

$\rho$ density

$\varphi$ energy thickness

Subscripts:

ad based on adiabatic wall conditions

D based on local diameter

r based on reference temperature

s static condition

t stagnation condition

w wall condition

z axial distance from nozzle entrance

$\theta$ based on momentum thickness

$\varphi$ based on energy thickness

$\infty$ condition in the free stream

0 stagnation condition in plenum

Superscripts:

* geometric throat value

## APPARATUS

The data of references 1 and 3 were obtained at a nominal stagnation temperature of 539 K and pressure of 207 $N/cm^2$ absolute in the facility at the NASA Lewis Research Center. This facility consisted of a heat exchanger, diffuser, plenum, pipe inlet, and nozzle as shown in figure 1. The heated air was passed into an exhaust system having a nominal pressure of 1.4 $N/cm^2$ absolute.

The test configurations comprised 16.5-centimeter-diameter uncooled (adiabatic-wall) as well as cooled pipe inlets coupled to water-cooled $30^{\circ}$ and $60^{\circ}$ half-angle of convergence by $15^{\circ}$ half-angle of divergence nozzles (hereinafter referred to as simply the $30^{\circ}$-$15^{\circ}$ nozzle, etc.). Details concerning inlet design and dimensions can be obtained in reference 7. The water-cooled $30^{\circ}$-$15^{\circ}$ and $60^{\circ}$-$15^{\circ}$ nozzles had a nominal throat diameter and throat radius of curvature of 3.8 centimeters. The contraction area ratio given by the ratio of inlet-to-throat cross-section area was approximately 18.8. The $30^{\circ}$-$15^{\circ}$ and $60^{\circ}$-$15^{\circ}$ nozzle dimensions are presented in tables I and II, respectively.

The data of reference 2 were also obtained in a heated air facility. The test conditions selected for the present report correspond to test number 440 which was conducted at a stagnation temperature of 811 K and pressure of 172 $N/cm^2$. The inlet for this test was water cooled and had a diameter of 12.7 centimeters. The water-cooled nozzles had a $45^{\circ}$ half-angle of convergence and $15^{\circ}$ half-angle of divergence and 4.06-centimeter-diameter throat. The throat radius of curvature to diameter ratio was 0.313. The nominal contraction area ratio for this configuration was 19.8 or approximately the same as that of the $30^{\circ}$-$15^{\circ}$ and $60^{\circ}$-$15^{\circ}$ nozzles. The dimensions for the nozzle of reference 2 are presented in table III.

## INSTRUMENTATION

Since the instrumentation for the $30^{\circ}$-$15^{\circ}$ and $60^{\circ}$-$15^{\circ}$ nozzles has been described previously (e.g., refs. 1 and 3) only an abbreviated description will be provided herein. The instrumentation pertinent to the present report consisted of wall heat flux meters and wall pressure taps.

The local heat transfer rates, wall temperatures, and wall static pressures in the $30^{\circ}$-$15^{\circ}$ and $60^{\circ}$-$15^{\circ}$ nozzles were measured at the stations shown in tables I and II, respectively. These measurements were obtained by means of 0.318-centimeter-diameter Inconel heat flux meters and the use of the heat-conduction equation.

Similar measurements were obtained in the $45^{\circ}$-$15^{\circ}$ nozzle of reference 2; however, the heat transfer was obtained by a calorimetric technique involving the measurement of water flow rates and corresponding temperature differences in small circumferential passages along the nozzle. The measurements were obtained at the stations shown in table III.

## HEAT TRANSFER DATA REDUCTION

The nozzle heat transfer results will be presented in terms of the nondimensional grouping $St_r Pr^{0.7}$ which can be written as

$$St_r Pr^{0.7} = \frac{q}{\rho_r u_\infty C_p (T_{ad} - T_w)} Pr^{0.7} \tag{1}$$

The heat flux $q$ and wall temperature $T_w$ are determined from the temperature measurements on the heat flux meters. The expression for the adiabatic wall temperature $T_{ad}$ is

$$T_{ad} = T_s + \mathcal{R}(T_0 - T_s) \tag{2}$$

where the recovery factor $\mathcal{R}$ for a turbulent boundary layer is equal to $Pr^{1/3}$. The subscript $r$ denotes that properties were evaluated at the Eckert reference temperature $T_r$ (ref. 8) where

$$T_r = T_s + 0.5(T_w - T_s) + 0.22\,\mathcal{R}(T_0 - T_s) \tag{3}$$

A Prandtl number of 0.71 was assumed in the previous equations.

## EXPERIMENTAL RESULTS

The data used in evaluating the predictive capabilities of the integral boundary layer theory of reference 5 and the modified analysis presented herein were selected in order to emphasize differences in inlet wall cooling, unit Reynolds number, and nozzle convergence conditions. The test cases which were examined are as follows:

(1) $30^\circ$-$15^\circ$ nozzle; $T_0 = 539$ K
  (a) Adiabatic inlet, $P_0 = 207$ N/cm$^2$ (ref. 3)
  (b) Cooled inlet, $P_0 = 207$ N/cm$^2$ (ref. 1)
  (c) Adiabatic inlet, $P_0 = 110$ N/cm$^2$ (ref. 3)
  (d) Cooled inlet, $P_0 = 110$ N/cm$^2$ (ref. 1)

(2) $60^\circ$-$15^\circ$ nozzle; $T_0 = 539$ K
  (a) Adiabatic inlet, $P_0 = 207$ N/cm$^2$ (ref. 3)
  (b) Cooled inlet, $P_0 = 207$ N/cm$^2$ (ref. 1)

(3) $45^\circ$-$15^\circ$ nozzle; $T_0 = 811$ K; cooled inlet, $P_0 = 172$ N/cm$^2$ (ref. 2)

The Reynolds numbers resulting from the previous test conditions are considered to be sufficient to produce a turbulent boundary layer in the nozzles in contrast to a "laminarized" boundary layer which was discussed in references 1 and 2.

The experimental values of the Mach number, wall temperature, and heat transfer for the three nozzles are tabulated in tables IV to VI. These basic quantities can be used to convert the heat transfer which is expressed as $St_r Pr^{0.7}$ to other commonly used heat transfer parameters.

The experimental heat transfer $St_r Pr^{0.7}$ is plotted as a function of the axial distance $x/D^*$ in figures 2 to 8. In all cases a minimum in $St_r Pr^{0.7}$ can be noted at or near the geometric throat. This minimum in $St_r Pr^{0.7}$ is characteristic of the flow in converging-diverging nozzles. This effect has been observed to be as low as 50 percent of the value of $St_r Pr^{0.7}$ for unaccelerated flow at the same value of $Re_D$ and fixed free stream conditions (refs. 1 to 4).

The effects of altering the inlet cooling, nozzle convergence angle, and Reynolds number on the nozzle heat transfer were reviewed in reference 7 and therefore, will merely be summarized herein. The effects of inlet cooling can be observed by comparing figures 2 and 3 for the $30^\circ$-$15^\circ$ nozzle or figures 4 and 5 for the $60^\circ$-$15^\circ$ nozzle. In both nozzles, the local heat transfer in tests with the cooled inlet is always lower than values corresponding to tests with the uncooled inlet. The increase in inlet cooling increased the value of the boundary layer energy thickness $\varphi$ at the nozzle entrance and also decreased the nozzle wall temperature (refer to tables IV and V).

The effects of nozzle convergence angle on the heat transfer for the same inlet cooling can best be illustrated by comparing the throat values of $St_r Pr^{0.7}$ in the $30^\circ$-$15^\circ$ and $60^\circ$-$15^\circ$ nozzles since the throat Reynolds numbers were approximately equal. A comparison of the results in figures 2 and 6 or figures 3 and 7 reveals that an increase in convergence angle and, hence, a change in the free stream velocity distribution results in higher values of throat heat transfer. This indicates the importance of the accelerated boundary layer history.

A reduction in stagnation pressure and, consequently, a reduction in Reynolds number tends to increase the value of $St_r Pr^{0.7}$ at a given station in the nozzle. This can be noted by comparing the results for the $30^\circ$-$15^\circ$ nozzle in figures 4 and 5 for a stagnation pressure of 110 N/cm$^2$ with the corresponding results in figures 2 and 3 for a stagnation pressure of 207 N/cm$^2$. The observed trend is predictable on the basis of simple heat transfer relations for unaccelerated flow which indicate that $St_r Pr^{0.7}$ varies approximately as $Re_D^{-0.2}$ (or as $P_0^{-0.2}$ for the data in figs. 2 to 5). Therefore, upon reducing the pressure from 207 to 110 N/cm$^2$ an increase of about 12 percent in $St_r Pr^{0.7}$ would be expected. The data tend to be quantitatively consistent with this result.

## PREDICTED RESULTS

As mentioned previously, the energy method provided good estimates of throat heat transfer; however, in many applications it is also desirable to improve the predictions of heat transfer in the entrance and exit portions of the nozzle. The fundamental criteria set forth by the heat transfer data are as follows: (1) the method must predict the heat transfer at the nozzle entrance (onset of acceleration) and thus reflect the upstream history which, in the present study, was dictated by pipe inlet geometry and cooling, (2) the method must account for the differences in local heat transfer resulting from different levels of acceleration as manifested in the nozzle convergence angle, and (3) the method must account for the effects of Reynolds number on the heat transfer.

With the aforementioned criteria in mind, it is first desirable to review the predictions of heat transfer based on the original formulation of the energy method of reference 5. The method of reference 5 involves the solution of the integral momentum and energy equations and employs Coles friction law, 1/7-power profiles for the velocity and temperature difference ratios, and a modified von Kármán form of Reynolds analogy. Details of the method which are pertinent to the present study are given in the appendix.

### Application of the Theory of Reference 5

The predicted heat transfer based on the energy method of reference 5 ($N = 0$ in eq. (A1)) is shown for the $30^{\circ}$-$15^{\circ}$ and $60^{\circ}$-$15^{\circ}$ nozzles in figures 2 to 7 and for the $45^{\circ}$-$15^{\circ}$ nozzle (ref. 2) in figure 8. All of the calculations were initialized at the nozzle entrance. The initial values of the boundary layer thicknesses $\delta$ and $\Delta$ for the tests with cooled inlets (figs. 3, 5, 7, and 8) were obtained by computation from measured values in the pipe inlets using the method of reference 5.

The value of $\Delta$ in the nozzle entrance for tests with the uncooled inlet (figs. 2, 4, and 6) was determined by the procedure of reference 3. This procedure entailed varying the value of $(\Delta/\delta)_{z=0}$ until the calculations converged to the same value of throat heat transfer coefficient. Since the thermal boundary layer begins to develop at the nozzle entrance, the value of $\Delta/\delta$ at this station should be quite small. The value of $\Delta/\delta$ selected for the present data is the same value that was used in reference 3; namely, $(\Delta/\delta)_{z=0} = 0.01$.

Since, in the energy method, the heat transfer can be calculated independent of the momentum equation, the initial value of momentum thickness does not alter the predicted heat transfer rates. This result is reasonably consistent with the experimental data of reference 9. However, in the predicted results shown in figures 2 to 8, the basic shape of the theoretical distribution differs appreciably from the data. As shown in

reference 3, the energy method provides the best agreement with data in the throat region of the nozzle.

An alternate method of applying the theory is to assume that the interaction exponent N in equation (A1) has a value of 0.25. This is approximately equivalent to incorporating the standard form of the von Kármán momentum heat analogy since the friction coefficient for a turbulent boundary layer usually varies as $Re_{\theta}^{-0.25}$.

Predictions based on this alternate method are shown for the $30^{o}$-$15^{o}$ nozzle with the uncooled inlet in figure 2. Since the Stanton number in this option is a strong function of $Re_{\theta}$ which is much greater than $Re_{\varphi}$, large differences in predicted heat transfer in the entrance region are apparent. Obviously, predictions of the heat transfer from this option of the theory are not as good as the results based on the energy method (fig. 2).

One final consideration in the method of reference 5 concerns the 1/7-power-profile assumption for the temperature and velocity in the boundary layer. Although other power laws have been suggested in the literature, it was shown in reference 9 that the predicted heat transfer resulting from an energy calculation was insensitive to the power law assumption.

## Predicted Results Based on a Modification of the Theory of Reference 5

Significant improvements in the predicted heat transfer distribution could not be obtained by using different combinations of the options in the method of reference 5. The predicted heat transfer appears to depend principally on the form of the auxiliary equation which relates the Stanton number to an energy thickness Reynolds number function (eq. (A1)). In order to improve the predictions of heat transfer by the energy method, the limiting case of a pipe flow was considered. In a pipe-cone configuration the heat transfer in the entrance region of the nozzle ($du_{\infty}/dz \leq 0$) would be dictated in part by the length of pipe inlet preceding the convergent portion of the nozzle. For the Reynolds number levels and entrance conditions of the present nozzles, an expression for the Stanton number which generally improved the agreement with the data in the nozzle entrance region (where the velocity gradient is approximately zero) was determined to be

$$St = 1.6\, f(Re_{\varphi}) \tag{4}$$

where the Reynolds number function is

$$f(Re_\varphi) = \frac{\frac{C_f(Re_\varphi)}{2}}{1 - 5\left[\frac{C_f(Re_\varphi)}{2}\right]^{1/2}\left[1 - Pr + \ln\left(\frac{6}{5Pr + 1}\right)\right]} \tag{5}$$

As the flow accelerates in the convergent portion of the nozzle, the heat transfer is attenuated from the pipe flow level. Upon examining several nondimensional acceleration parameters it was empirically determined that the heat transfer could be correlated in terms of $f(Re_\varphi)$ and the acceleration parameter $S\, d(\ln u_\infty R)/dS$, resulting in the following expression for the Stanton number:

$$St = 1.6f(Re_\varphi)\left[1.0 - 0.11S\frac{d(\ln u_\infty R)}{dS}\right] \tag{6}$$

The length $S$ is measured along the wall starting at the nozzle entrance. The constant of 0.11 in equation (6) was determined by matching the predicted results to the $30^\circ$-$15^\circ$ nozzle data in figure 2.

The Stanton number in equation (9) was quite sensitive to the acceleration parameter $S\, d(\ln u_\infty R)/dS$; therefore, it was found desirable to smooth the $\ln u_\infty R$ term before performing the numerical differentiation. Each smooth value of $\ln u_\infty R$ was obtained by evaluating at the corresponding distance $z$ the least square polynomial of degree one relevant to $z$ and the two adjacent points. The numerical differentiation was performed by means of a spline-fit technique.

The results in figures 2 to 8 indicate that, in general, the modified analysis yields a better distribution of heat transfer than the original analysis of reference 5, particularly downstream of the throat. The local heat transfer prediction near the nozzle entrance appears to be greatly improved in the tests with cooled inlets (figs. 3, 5, 7, and 8). No improvement over the reference 5 method is apparent for the cases in which uncooled inlets were used (figs. 2, 4, and 6); however, in the latter cases, the shape of the distribution in the subsonic portion of the nozzle is generally more consistent with the data when based on the modified analysis.

In the majority of cases an improvement in the prediction of the throat heat transfer is apparent with the use of the modified analysis. The throat data in figure 4, corresponding to the $30^\circ$-$15^\circ$ nozzle uncooled inlet configuration operating at $P_0 = 110$ N/cm$^2$, are in better agreement with the results based on the method of reference 5.

## Integrated Heat Transfer in the Nozzle

The total heat flux in the nozzle can be determined by integrating the local values of q over the nozzle surface area as shown by the following equation:

$$Q = \int^{A} q \, dA \tag{7}$$

Equation (7) can be expressed in terms of the $St_r Pr^{0.7}$ grouping and the axial distance from the inlet z as

$$Q(z) = \frac{2\pi}{Pr^{0.7}} \int_0^z St_r Pr^{0.7} \rho_r u_\infty R C_p (T_{ad} - T_w) \left[1.0 + \left(\frac{dR}{dz}\right)^2\right]^{1/2} dz \tag{8}$$

where the Prandtl number Pr is assumed to be constant.

Values of the total heat transfer from the inlet to the throat $Q^*$ and from the inlet to the downstream station $Q_T$ are tabulated in table VII for the seven nozzle flows considered in this study.

The results in table VII indicate that the modified analysis generally overpredicts the integrated heat transfer from the nozzle entrance to the throat $Q^*$, whereas the method of reference 5 tended to underpredict $Q^*$. The differences in predicted values of $Q^*$ are insufficient to preclude one method in favor of the other. This result is especially interesting in the cases which had cooled inlets coupled to the nozzles, since, as shown previously, the modified analysis provided better agreement with the entrance values of $St_r Pr^{0.7}$ and approximately equal or better predictions of throat heat transfer. The underprediction of entrance heat transfer in these cases is offset by the overprediction in the throat of the nozzle so that the method of reference 5 provides good estimates of the integrated subsonic heat transfer. With the exception of the $45^\circ$-$15^\circ$ nozzle data the agreement in $Q^*$ was within 15 percent. In the latter data, the method of reference 5 underpredicted $Q^*$ by 24 percent. The maximum overprediction by the modified theory was 18 percent.

The modified theory provided better agreement with experimental values of total heat transfer $Q_T$ (integrated heat transfer from the nozzle entrance to exit station) in all cases except for the $60^\circ$-$15^\circ$ nozzle and cooled inlet configuration operating at $P_0 = 207$ $N/cm^2$ (fig. 7). In this latter case the modified theory overpredicted the experimental values of $Q_T$ by 16 percent. In all of the other cases the agreement was within 6 per-

cent. The method of reference 5 tended to underestimate the total heat transfer by from 8 to 26 percent.

## SUMMARY OF RESULTS

An integral turbulent boundary layer theory was applied to heat transfer data from previous studies with heat air in $30^{\circ}$-$15^{\circ}$, $45^{\circ}$-$15^{\circ}$, and $60^{\circ}$-$15^{\circ}$ water-cooled nozzles. In general, improved predictions of local heat transfer and consequently the total or integrated heat transfer in the nozzles were obtained by modifying the momentum-heat analogy (auxiliary equation in the standard energy analysis). It was proposed that the original equation, $St = f(Re_{\varphi})$, be replaced by the following expression for the Stanton number:

$$St = 1.6\, f(Re_{\varphi})\left[1.0 - 0.11S\frac{d(\ln u_{\infty} R)}{dS}\right]$$

where St is the Stanton number, $Re_{\varphi}$ is the Reynolds number based on energy thickness, S is the distance along the wall starting from the cone entrance, $u_{\infty}$ is the velocity in the free stream, and R is the local radius. The predicted results indicated the following:

1. When the original theory ($St = f(Re_{\varphi})$) was applied to data in which cooled inlets were coupled to the cooled nozzles, an underprediction of the nozzle entrance and exit heat transfer and overprediction of throat heat transfer resulted. The modified theory generally provided better estimates of local heat transfer throughout the nozzle. Although the original method provided better estimates of heat transfer in the nozzle entrance region for the tests in which uncooled inlets were coupled to the cooled nozzles, the modified theory generally predicted a subsonic nozzle heat transfer distribution more consistent with the data. A pronounced improvement in nozzle exit values of predicted heat transfer was obtained when the modified theory was used.

2. The integrated heat transfer in the subsonic portion of the nozzle was generally greater than experimental values when the modified theory was used and less than experimental values when the original analysis was employed. Although the original theory often underpredicted the local heat transfer in the nozzle entrance region and overpredicted the throat heat transfer, the integrated heat transfer in the subsonic portion of the nozzle was within about 15 percent of the data because of these compensating effects.

A pronounced improvement in the agreement between predicted and experimental total heat transfer in the nozzle was obtained when the modified theory was used. With the exception of one case the total heat transfer in the nozzle was within 6 percent of the

experimental values. The original energy analysis generally provided agreement within 18 percent of the integrated values of experimental heat transfer. Estimates of total heat transfer from the latter method were always less than the experimental values.

Lewis Research Center,
National Aeronautics and Space Administration,
Cleveland, Ohio, December 13, 1971,
132-15.

# APPENDIX - REVIEW OF BOUNDARY LAYER THEORY OF REFERENCE 5

The boundary layer theory of reference 5 involves the simultaneous solution of the integral momentum and energy equations in conjunction with auxiliary relations for the skin friction coefficient, boundary layer velocity and temperature profiles, and momentum-heat analogy. All predictions of heat transfer which are based on the method of reference 5 will incorporate the following relations for these auxiliary conditions.

## Skin Friction Coefficient

The skin friction coefficient $C_f$ was determined by assuming that it was equal to the adiabatic value $C_{f,ad}$ obtained when $T_w = T_{ad}$. The value of $C_{f,ad}$ was determined by the method of Coles (see ref. 5 for details).

## Interaction Exponent

An interaction exponent N is used to relate the Stanton number for unequal momentum and energy thickness to that for equal thickness by means of a factor $(\varphi/\theta)^N$ as shown in the following equation:

$$St = \frac{\frac{C_f(Re_\varphi)}{2}\left(\frac{\varphi}{\theta}\right)^N}{1 - 5\left[\frac{C_f(Re_\varphi)}{2}\right]^{1/2}\left[1 - Pr + \ln\left(\frac{6}{5\,Pr + 1}\right)\right]} \tag{A1}$$

When $\varphi = \theta$, equation (A1) reduces to the familiar von Kármán form of Reynolds analogy. When N = 0, equation (A1) can be solved in conjunction with the integral energy equation for the Stanton number. In the present study the interaction exponent N will have a value of zero (energy calculation) unless otherwise specified.

## Power Law

The 1/7-power law assumption in the method of reference 5 which apply to the velocity and temperature difference ratios are

$$\frac{u}{u_\infty} = \left(\frac{y}{\delta}\right)^{1/7} \tag{A2}$$

$$\frac{(T_t - T_w)}{(T_0 - T_w)} = \left(\frac{y}{\Delta}\right)^{1/7} \tag{A3}$$

## REFERENCES


1. Boldman, Donald R.; Schmidt, James F.; and Gallagher, Anne K.: Laminarization of a Turbulent Boundary Layer as Observed from Heat-Transfer and Boundary-Layer Measurements in Conical Nozzles. NASA TN D-4788, 1968.

2. Back, L. H.; Massier, P. F.; and Cuffel, R. F.: Flow Phenomena and Convective Heat Transfer in a Conical Supersonic Nozzle. J. Spacecraft Rockets, vol. 4, no. 8, Aug. 1967, pp. 1040-1047.

3. Boldman, Donald R.; Neumann, Harvey E.; and Schmidt, James F.: Heat Transfer in $30^{\circ}$ and $60^{\circ}$ Half-Angle of Convergence Nozzles with Various Diameter Uncooled Pipe Inlets. NASA TN D-4177, 1967.

4. Graham, Robert W.; and Boldman, Donald R.: The Use of Energy Thickness in Prediction of Throat Heat Transfer in Rocket Nozzles. NASA TN D-5356, 1969.

5. Bartz, D. R.: Turbulent Boundary-Layer Heat Transfer from Rapidly Accelerating Flow of Rocket Combustion Gases and of Heated Air. Advances in Heat Transfer. Vol. 2. James P. Hartnett and Thomas F. Irvine, Jr., eds., Academic Press, 1965, pp. 1-108.

6. Schmidt, James F.; Boldman, Donald R.; and Todd, Carroll: Similar Solutions for Turbulent Boundary Layer with Large Favorable Pressure Gradients (Nozzle Flow with Heat Transfer). NASA TN D-6439, 1971.

7. Boldman, Donald R.; and Graham, Robert W.: Heat Transfer and Boundary Layer in Conical Nozzles. NASA TN D-6594, 1971.

8. Eckert, E. R. G.; and Drake, Robert M., Jr.: Heat and Mass Transfer. Second ed., McGraw-Hill Book Co., Inc., 1959.

9. Boldman, D. R.; Schmidt, J. F.; and Ehlers, R. C.: Effect of Uncooled Inlet Length and Nozzle Convergence Angle on the Turbulent Boundary Layer and Heat Transfer in Conical Nozzles Operating with Air. J. Heat Transfer, vol. 89, no. 4, Nov. 1967, pp. 341-350.

TABLE I. - INSTRUMENTATION SITES FOR 30°-15° NOZZLE

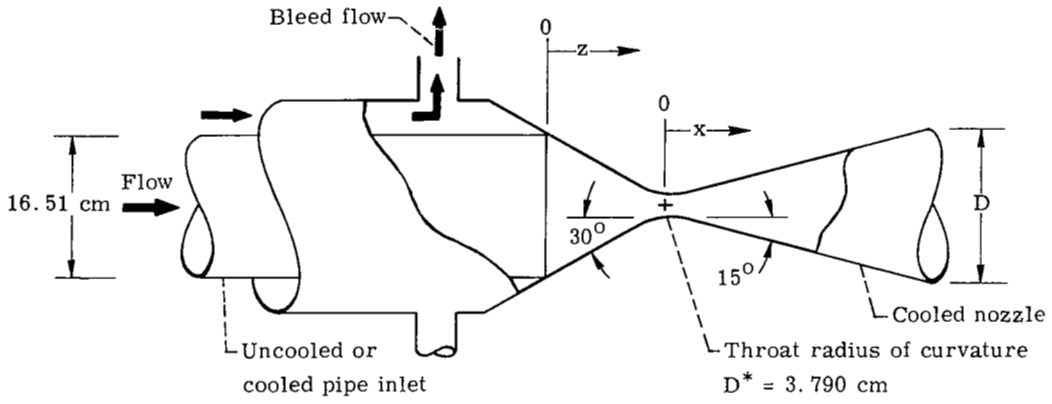


| Station | Axial distance from nozzle entrance, z, cm | Axial distance from nozzle throat, x, cm | Diameter, D, cm | Nondimensional distance from nozzle throat, $x/D^*$ |
|---|---|---|---|---|
| Entrance | 0 | -12.032 | 16.510 | -3.175 |
| 1 | .564 | -11.468 | 15.875 | -3.026 |
| 2 | 3.104 | -8.928 | 12.934 | -2.356 |
| 3 | 5.652 | -6.380 | 9.992 | -1.684 |
| 4 | 6.551 | -5.481 | 8.961 | -1.446 |
| 5 | 7.430 | -4.602 | 7.945 | -1.214 |
| 6 | 8.324 | -3.708 | 6.914 | -.979 |
| 7 | 9.213 | -2.819 | 5.883 | -.744 |
| 8 | 10.475 | -1.557 | 4.470 | -.411 |
| 9 | 11.587 | -.445 | 3.835 | -.117 |
| 10 | 12.032 | 0 | 3.790 | 0 |
| 11 | 12.362 | .330 | 3.815 | .087 |
| 12 | 12.680 | .648 | 3.912 | .171 |
| 13 | 13.028 | .996 | 4.074 | .263 |
| 14 | 13.642 | 1.610 | 4.399 | .425 |
| 15 | 15.133 | 3.101 | 5.187 | .818 |
| 16 | 18.981 | 6.949 | 7.259 | 1.834 |
| 17 | 25.921 | 13.889 | 10.978 | 3.665 |

TABLE II. - INSTRUMENTATION SITES FOR $60^{o}$-$15^{o}$ NOZZLE

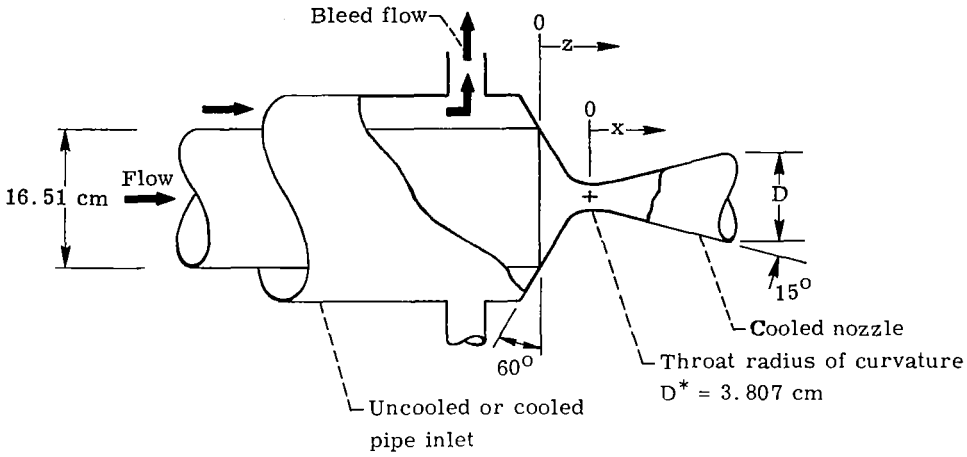


| Station | Axial distance from nozzle entrance, z, cm | Axial distance from nozzle throat, x, cm | Diameter, D, cm | Nondimensional distance from nozzle throat, $x/D^*$ |
|---|---|---|---|---|
| Entrance | 0 | -5.852 | 16.510 | -1.537 |
| 1 | .556 | -5.296 | 14.580 | -1.391 |
| 2 | 1.402 | -4.450 | 11.643 | -1.169 |
| 3 | 1.699 | -4.153 | 10.612 | -1.091 |
| 4 | 2.004 | -3.848 | 9.555 | -1.011 |
| 5 | 2.789 | -3.063 | 6.939 | -.805 |
| 6 | 3.261 | -2.591 | 5.865 | -.680 |
| 7 | 4.376 | -1.476 | 4.409 | -.388 |
| 8 | 5.481 | -.371 | 3.851 | -.097 |
| 9 | 5.852 | 0 | 3.807 | 0 |
| 10 | 6.233 | .381 | 3.863 | .100 |
| 11 | 6.556 | .704 | 3.975 | .185 |
| 12 | 6.868 | 1.016 | 4.122 | .267 |
| 13 | 7.432 | 1.580 | 4.422 | .415 |
| 14 | 8.923 | 3.071 | 5.215 | .807 |
| 15 | 11.288 | 5.436 | 6.464 | 1.428 |

TABLE III. - INSTRUMENTATION SITES FOR

$45^{o}$-$15^{o}$ NOZZLE (REF. 2)

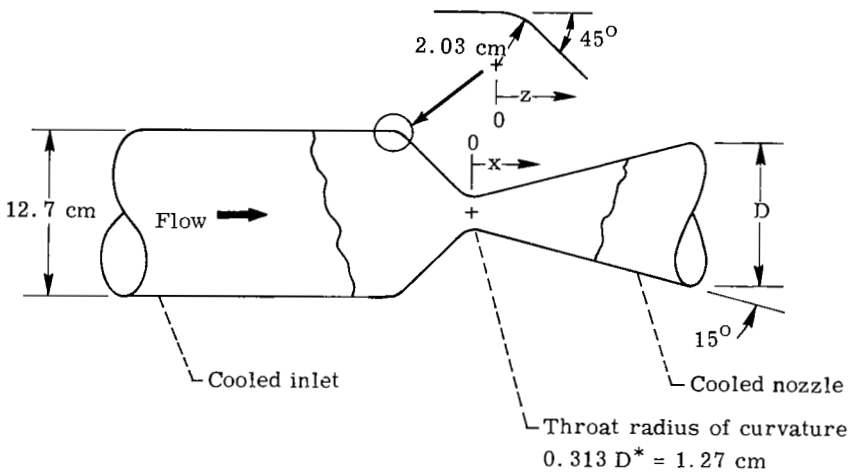


| Station | Axial distance from nozzle entrance, z, cm | Axial distance from nozzle throat, x, cm | Diameter, D, cm | Nondimensional distance from nozzle throat, $x/D^*$ |
|---|---|---|---|---|
| Entrance | 0 | -5.687 | 12.715 | -1.399 |
| 1 | .320 | -5.367 | 12.620 | -1.321 |
| 2 | .955 | -4.732 | 12.216 | -1.164 |
| 3 | 1.468 | -4.219 | 11.400 | -1.038 |
| 4 | 1.961 | -3.726 | 10.441 | -.917 |
| 5 | 2.428 | -3.259 | 9.523 | -.802 |
| 6 | 2.893 | -2.794 | 8.585 | -.688 |
| 7 | 3.358 | -2.329 | 7.654 | -.573 |
| 8 | 3.823 | -1.864 | 6.742 | -.459 |
| 9 | 4.247 | -1.440 | 5.873 | -.354 |
| 10 | 4.625 | -1.062 | 5.119 | -.261 |
| 11 | 5.083 | -.604 | 4.365 | -.149 |
| 12 | 5.682 | -.005 | 4.064 | -.001 |
| 13 | 6.368 | .681 | 4.320 | .168 |
| 14 | 7.155 | 1.468 | 4.760 | .361 |
| 15 | 7.973 | 2.286 | 5.195 | .563 |
| 16 | 8.832 | 3.145 | 5.662 | .774 |
| 17 | 10.145 | 4.458 | 6.377 | 1.097 |
| 18 | 11.872 | 6.185 | 7.307 | 1.522 |
| 19 | 13.584 | 7.897 | 8.229 | 1.943 |
| 20 | 15.281 | 9.594 | 9.149 | 2.361 |

TABLE IV. - TABULATED HEAT TRANSFER DATA FOR $30^{\circ}$-$15^{\circ}$ NOZZLE

[Throat diameter $D^*$ = 3.790 cm.]

| Station | Nondimensional distance from nozzle throat, $x/D^*$ | Mach number, M | Uncooled inlet (ref. 3) | | | | Cooled inlet (ref. 1) | | | |
|---|---|---|---|---|---|---|---|---|---|---|
| | | | Stagnation pressure $P_0$ = 206.5 N/cm$^2$; Stagnation temperature $T_0$ = 538.8 K | | Stagnation pressure $P_0$ = 108.8 N/cm$^2$; Stagnation temperature, $T_0$ = 539.2 K | | Stagnation pressure $P_0$ = 205.6 N/cm$^2$; Stagnation temperature, $T_0$ = 537.9 K | | Stagnation pressure $P_0$ = 109.8 N/cm$^2$; Stagnation temperature $T_0$ = 540.0 K | |
| | | | Wall temperature, $T_w$, K | Heat transfer, $St_r Pr^{0.7}$ | Wall temperature, $T_w$, K | Heat transfer $St_r Pr^{0.7}$ | Wall temperature, $T_w$, K | Heat transfer, $St_r Pr^{0.7}$ | Wall temperature, $T_w$, K | Heat transfer, $St_r Pr^{0.7}$ |
| Entrance | -3.175 | 0.02361 | 388.9 | ---------- | 363.9 | ---------- | 374.4 | ---------- | 364.4 | ---------- |
| 1 | -3.026 | .02778 | 389.8 | $0.264\times10^{-2}$ | 363.6 | $0.305\times10^{-2}$ | 376.2 | $0.172\times10^{-2}$ | 365.9 | $0.203\times10^{-2}$ |
| 2 | -2.356 | .04678 | 395.3 | .180 | 361.4 | .177 | 389.3 | .138 | 367.9 | .136 |
| 3 | -1.684 | .07894 | 423.9 | .174 | 378.7 | .145 | 419.6 | .138 | 387.6 | .118 |
| 4 | -1.446 | .09841 | 433.3 | .161 | 391.4 | .147 | 423.8 | .125 | 396.2 | .119 |
| 5 | -1.214 | .1266 | 440.3 | .146 | 403.4 | .144 | 427.7 | .106 | 405.4 | .112 |
| 6 | -.979 | .1684 | 447.9 | .125 | 415.0 | .135 | 434.6 | $.915\times10^{-3}$ | 415.1 | .102 |
| 7 | -.744 | .2347 | 457.8 | .119 | 428.3 | .132 | 444.4 | .868 | 425.2 | $.992\times10^{-3}$ |
| 8 | -.411 | .5055 | 470.5 | $.819\times10^{-3}$ | 447.6 | .104 | 456.9 | .573 | 441.7 | .696 |
| 9 | -.117 | .9281 | 465.3 | .673 | 448.2 | $.887\times10^{-3}$ | 457.3 | .527 | 443.3 | .642 |
| 10 | 0 | 1.1144 | 461.6 | .655 | 444.9 | .911 | 457.7 | .542 | 440.2 | .629 |
| 11 | .087 | 1.2751 | 457.9 | .737 | 442.2 | .967 | 445.9 | .464 | 434.2 | .628 |
| 12 | .171 | 1.4846 | 454.7 | .803 | 432.1 | .940 | 441.3 | .505 | 429.4 | .677 |
| 13 | .263 | 1.6811 | 449.4 | .923 | 425.1 | $.105\times10^{-2}$ | 436.7 | .608 | 423.2 | .756 |
| 14 | .425 | 1.7706 | 443.8 | .880 | 419.1 | .101 | 434.5 | .627 | 419.8 | .760 |
| 15 | .818 | 2.0818 | 431.3 | $.100\times10^{-2}$ | 406.0 | .114 | 424.8 | .770 | 408.6 | .894 |
| 16 | 1.834 | 2.7889 | 403.2 | .153 | 370.3 | .147 | 397.8 | $.117\times10^{-2}$ | 379.2 | $.126\times10^{-2}$ |
| 17 | 3.665 | 3.7392 | 345.0 | .158 | 327.1 | .167 | 350.5 | .149 | 341.3 | .156 |

TABLE V. - TABULATED HEAT TRANSFER DATA FOR $60^{\circ}$-$15^{\circ}$ NOZZLE

[Throat diameter $D^*$ = 3.807 cm.]

| Station | Nondimensional distance from nozzle throat, $x/D^*$ | Mach number, M | Uncooled inlet (ref. 3) | | Cooled inlet (ref. 1) | |
|---|---|---|---|---|---|---|
| | | | Stagnation pressure $P_0$ = 207.0 N/cm$^2$; Stagnation temperature $T_0$ = 537.7 K | | Stagnation pressure $P_0$ = 207.1 N/cm$^2$; Stagnation temperature $T_0$ = 539.6 K | |
| | | | Wall temperature, $T_w$, K | Heat transfer, $St_r Pr^{0.7}$ | Wall temperature, $T_w$, K | Heat transfer, $St_r Pr^{0.7}$ |
| Entrance | -1.537 | 0.01800 | 383.9 | ---------- | 385.6 | ---------- |
| 1 | -1.391 | .02300 | 384.4 | $0.340\times10^{-2}$ | 388.8 | $0.233\times10^{-2}$ |
| 2 | -1.169 | .03646 | 387.9 | .234 | 396.3 | .173 |
| 3 | -1.091 | .04989 | 392.2 | .190 | 400.3 | .142 |
| 4 | -1.011 | .06651 | 402.2 | .166 | 406.3 | .122 |
| 5 | -.805 | .1652 | 440.4 | .130 | 434.1 | $.842\times10^{-3}$ |
| 6 | -.680 | .2544 | 460.6 | .125 | 454.2 | .810 |
| 7 | -.388 | .5356 | 473.1 | .109 | 470.9 | .749 |
| 8 | -.097 | .9366 | 476.8 | $.990\times10^{-3}$ | 469.6 | .601 |
| 9 | 0 | 1.1004 | 474.9 | $.102\times10^{-2}$ | 467.7 | .605 |
| 10 | .100 | 1.3471 | 470.3 | .118 | 461.1 | .643 |
| 11 | .185 | 1.5289 | 463.1 | .121 | 457.9 | .763 |
| 12 | .267 | 1.6384 | 457.1 | .111 | 453.9 | .788 |
| 13 | .415 | 1.7907 | 445.9 | .112 | 445.1 | .805 |
| 14 | .807 | 2.0944 | 429.1 | .121 | 431.8 | .933 |
| 15 | 1.428 | 2.5460 | 406.1 | .136 | 414.5 | $.102\times10^{-2}$ |

TABLE VI. - TABULATED HEAT TRANSFER DATA

FOR $45^{\circ}$-$15^{\circ}$ NOZZLE (REF. 2)

[Throat diameter $D^*$ = 4.064 cm.]

| Station | Nondimensional distance from nozzle throat, $x/D^*$ | Mach number, M | Cooled inlet | |
|---|---|---|---|---|
| | | | Stagnation pressure $P_0$ = 172.2 N/cm$^2$; Stagnation temperature $T_0$ = 811.1 K | |
| | | | Wall temperature, $T_w$, K | Heat transfer, $St_r Pr^{0.7}$ |
| Entrance | -1.399 | 0.01800 | 373.9 | $0.851\times10^{-3}$ |
| 1 | -1.321 | .02300 | 371.7 | .764 |
| 2 | -1.164 | .03646 | 373.9 | .982 |
| 3 | -1.038 | .05281 | 382.2 | 1.008 |
| 4 | -.917 | .06331 | 386.1 | 1.024 |
| 5 | -.802 | .09789 | 396.7 | .978 |
| 6 | -.688 | .1123 | 408.9 | 1.070 |
| 7 | -.573 | .1399 | 417.8 | 1.104 |
| 8 | -.459 | .1711 | 426.7 | 1.075 |
| 9 | -.354 | .1910 | 428.9 | .955 |
| 10 | -.261 | .3147 | 442.2 | .784 |
| 11 | -.149 | .7462 | 440.6 | .577 |
| 12 | -.001 | 1.3645 | 441.1 | .686 |
| 13 | .168 | 1.7321 | 437.8 | .729 |
| 14 | .361 | 1.8058 | 431.7 | .748 |
| 15 | .563 | 1.9234 | 430.0 | .771 |
| 16 | .774 | 2.0852 | 422.2 | .801 |
| 17 | 1.097 | 2.3427 | 416.1 | .742 |
| 18 | 1.522 | 2.6246 | 404.4 | .790 |
| 19 | 1.943 | 2.9429 | 396.7 | .917 |
| 20 | 2.361 | 3.1462 | 397.8 | .860 |

TABLE VII. - EXPERIMENTAL AND CALCULATED TOTAL HEAT TRANSFER IN NOZZLE

| Configuration | Figure showing heat transfer | Nominal stagnation temperature, $T_{0'}$ K | Nominal stagnation pressure, $P_{0'}$ N/cm$^2$ | Total heat transfer from inlet to throat, $Q^*$, kW | | | Ratio of calculated to experimental total heat transfer from inlet to throat | | Total heat transfer from inlet to downstream station, $Q_T$, kW | | | Ratio of calculated to experimental total heat transfer from inlet to downstream station | |
|---|---|---|---|---|---|---|---|---|---|---|---|---|---|
| | | | | Experiment | Theory (ref. 5) | Modified theory (present analysis) | Theory (ref. 5) | Modified theory (present analysis) | Experiment | Theory (ref. 5) | Modified theory (present analysis) | Theory (ref. 5) | Modified theory (present analysis) |
| [a]30°-15° nozzle, adiabatic inlet (ref. 3) | 2 | 539 | 207 | 5.16 | 4.82 | 6.10 | 0.93 | 1.18 | 8.60 | 7.35 | 9.01 | 0.85 | 1.05 |
| 30°-15° nozzle, cooled inlet (ref. 1) | 3 | | 207 | 4.17 | 3.55 | 4.68 | .85 | 1.12 | 6.98 | 5.69 | 7.21 | .82 | 1.03 |
| 30°-15° nozzle, adiabatic inlet (ref. 3) | 4 | | 110 | 3.77 | 3.58 | 4.05 | .95 | 1.07 | 6.27 | 5.50 | 6.19 | .88 | .99 |
| 30°-15° nozzle, cooled inlet (ref. 1) | 5 | | 110 | 2.83 | 2.53 | 3.33 | .89 | 1.17 | 4.83 | 4.06 | 5.13 | .84 | 1.06 |
| 60°-15° nozzle, adiabatic inlet (ref. 3) | 6 | | 207 | 3.07 | 2.70 | 3.05 | .88 | 1.00 | 4.61 | 3.98 | 4.55 | .86 | .99 |
| 60°-15° nozzle, cooled inlet (ref. 1) | 7 | | 207 | 2.22 | 2.03 | 2.59 | .91 | 1.17 | 3.36 | 3.09 | 3.90 | .92 | 1.16 |
| 45°-15° nozzle, cooled inlet (ref. 2) | 8 | 811 | 172 | 6.13 | 4.68 | 5.96 | .76 | .96 | 12.03 | 8.90 | 11.62 | .74 | .97 |

[a]Denotes configuration used to obtain constants in modified theory.

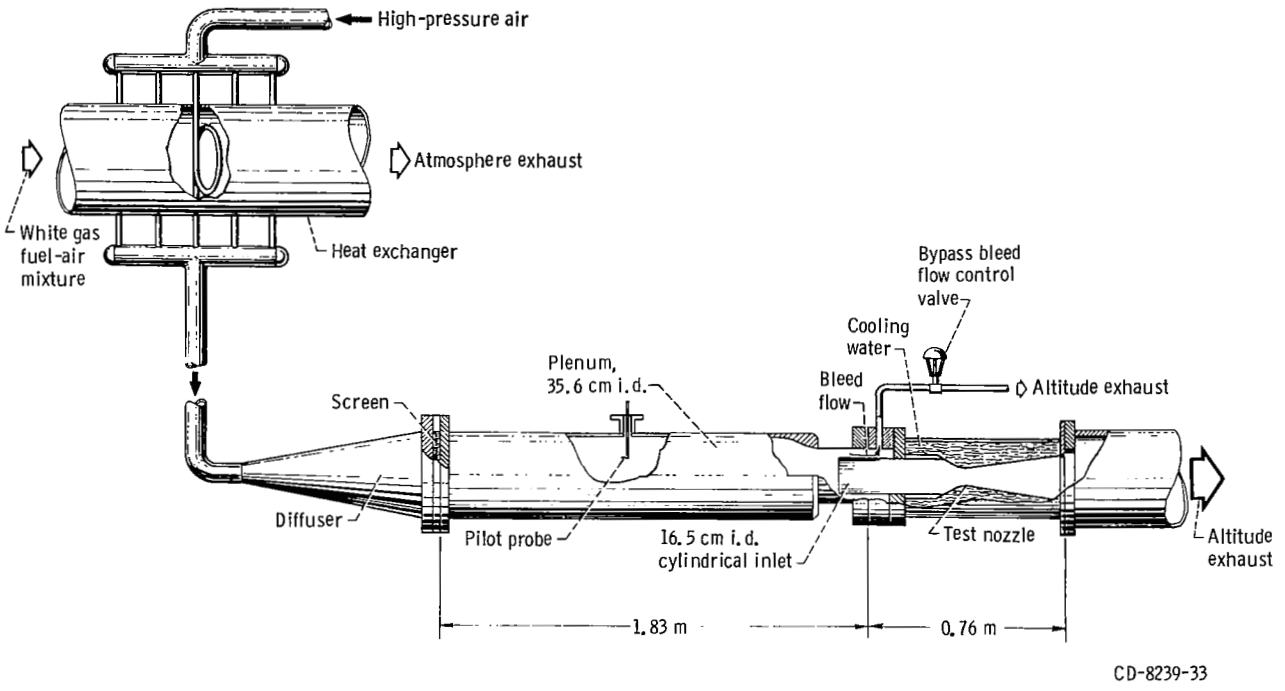


Figure 1. - Schematic diagram of NASA Lewis Research Center nozzle heat transfer facility.

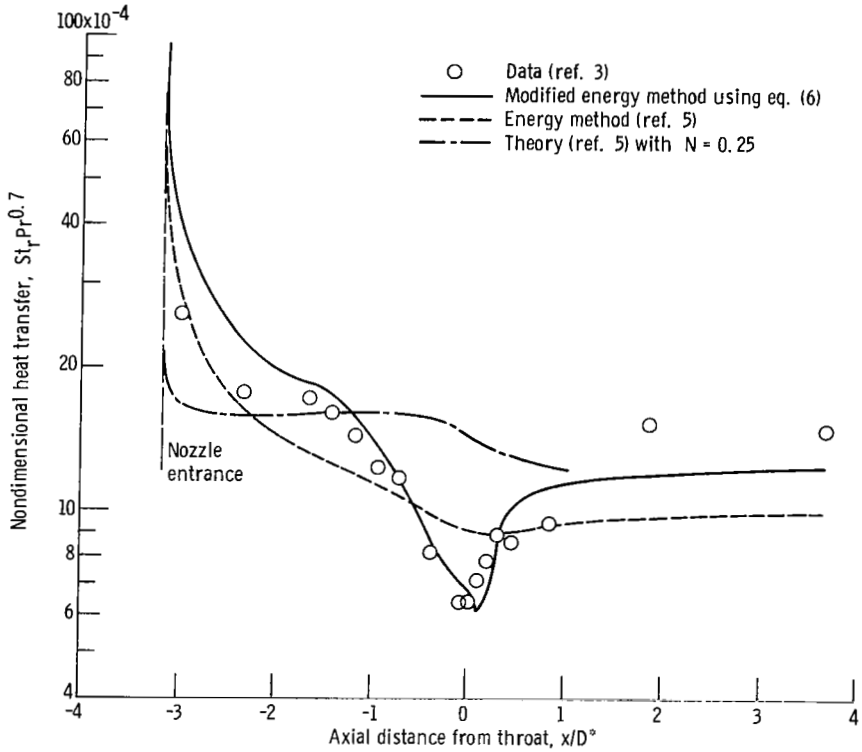


Figure 2. - Comparison of experimental and predicted heat transfer in $30^0$-$15^0$ nozzle operating with uncooled inlet. Stagnation temperature $T_0$ = 538.8 K; stagnation pressure $P_0$ = 206.5 N/cm$^2$; throat diameter $D^*$ = 3.790 centimeters. Deficiency thicknesses at nozzle entrance: energy thickness $\varphi$ = 0.000452 centimeter; momentum thickness $\theta$ = 0.0871 centimeter; displacement thickness $\delta^*$ = 0.106 centimeter.

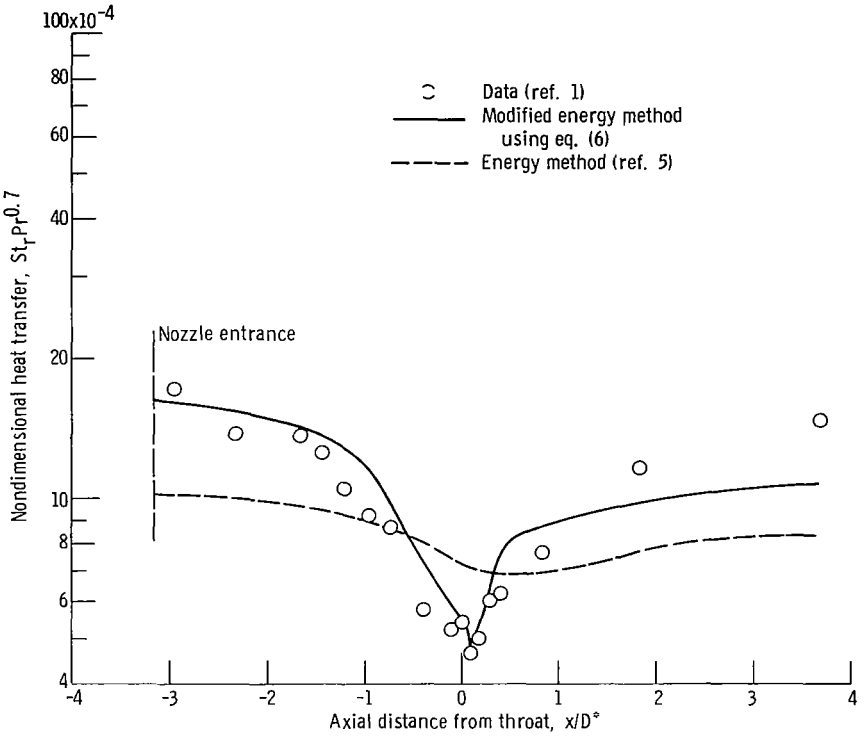


Figure 3. - Comparison of experimental and predicted heat transfer in $30^0$-$15^0$ nozzle operating with cooled inlet. Stagnation temperature $T_0$ = 537.9 K; stagnation pressure $P_0$ = 205.6 N/cm$^2$; throat diameter $D^*$ = 3.790 centimeters. Deficiency thicknesses at nozzle entrance: energy thickness $\varphi$ = 0.143 centimeter; momentum thickness $\theta$ = 0.160 centimeter; displacement thickness $\delta^*$ = 0.150 centimeter.

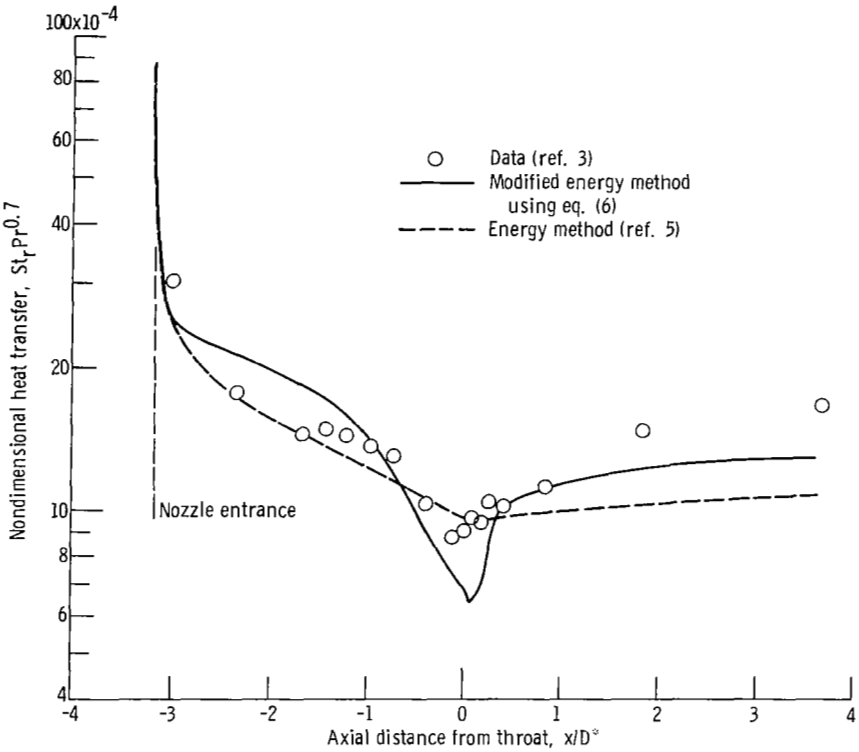


Figure 4. - Comparison of experimental and predicted heat transfer in $30^0$-$15^0$ nozzle operating with uncooled inlet. Stagnation temperature $T_0$ = 539.2 K; stagnation pressure $P_0$ = 108.8 N/cm$^2$; throat diameter $D^*$ = 3.790 centimeters. Deficiency thicknesses at nozzle entrance: energy thickness $\varphi$ = 0.000511 centimeter; momentum thickness $\theta$ = 0.0980 centimeter; displacement thickness $\delta^*$ = 0.118 centimeter.

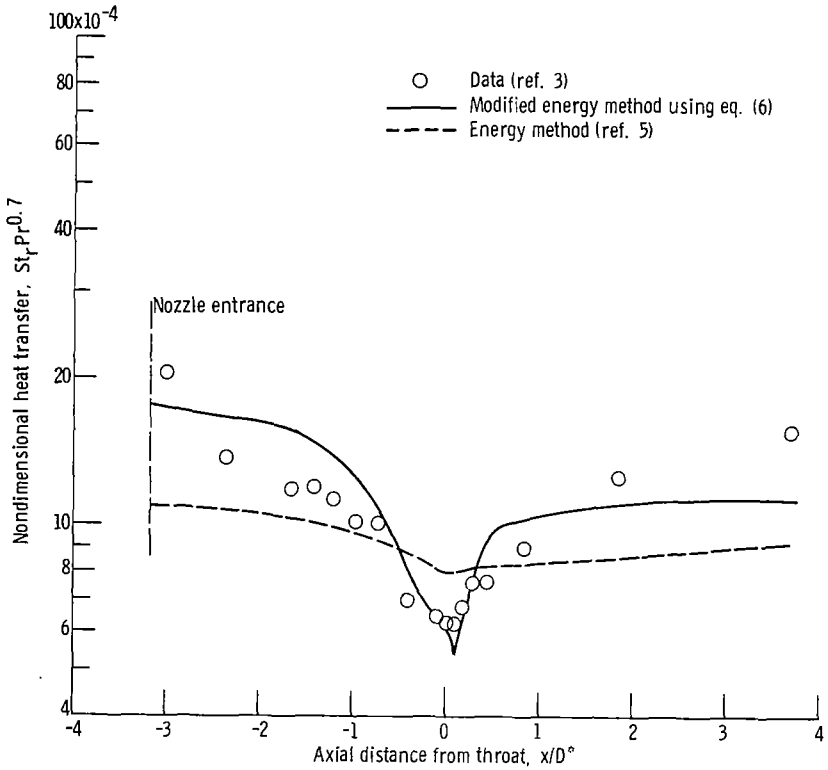


Figure 5. - Comparison of experimental and predicted heat transfer in $30^0$-$15^0$ nozzle operating with cooled inlet. Stagnation temperature $T_0$ = 540.0 K; stagnation pressure $P_0$ = 109.8 N/cm$^2$; throat diameter $D^*$ = 3.790 centimeters. Deficiency thicknesses at nozzle entrance: energy thickness $\varphi$ = 0.177 centimeter; momentum thickness $\theta$ = 0.194 centimeter; displacement thickness $\delta^*$ = 0.176 centimeter.

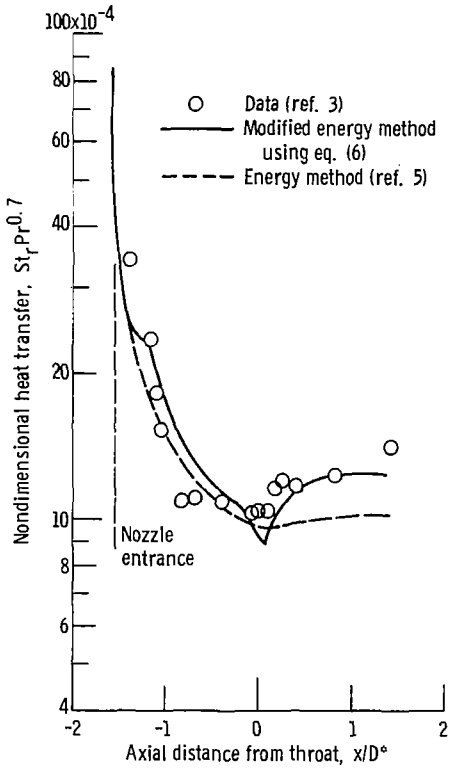


Figure 6. - Comparison of experimental and predicted heat transfer in $60^0$-$15^0$ nozzle operating with uncooled inlet. Stagnation temperature $T_0$ = 537.7 K; stagnation pressure $P_0$ = 207.0 N/cm$^2$; throat diameter $D^*$ = 3.807 centimeters. Deficiency thicknesses at nozzle entrance: energy thickness $\varphi$ = 0.000439 centimeter; momentum thickness $\theta$ = 0.000439 centimeter; displacement thickness $\delta^*$ = 0.000406 centimeter.

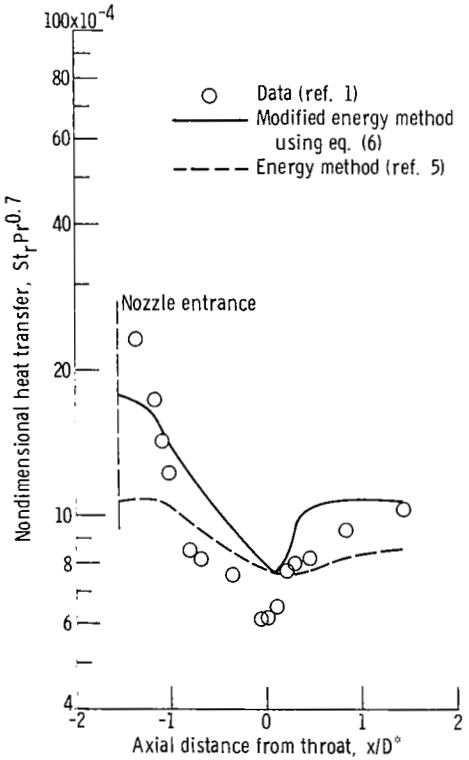


Figure 7. - Comparison of experimental and predicted heat transfer in $60^0$-$15^0$ nozzle operating with cooled inlet. Stagnation temperature $T_0$ = 539.6 K; stagnation pressure $P_0$ = 207.1 N/cm$^2$; throat diameter $D^*$ = 3.807 centimeters. Deficiency thicknesses at nozzle entrance: energy thickness $\varphi$ = 0.143 centimeter; momentum thickness $\theta$ = 0.160 centimeter; displacement thickness $\delta^*$ = 0.153 centimeter.

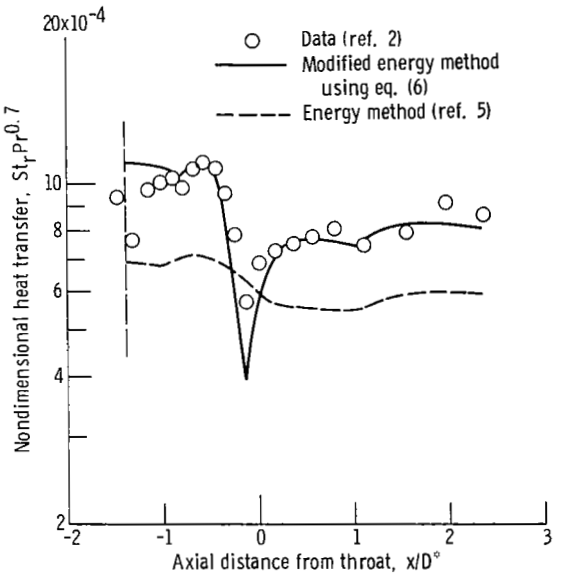


Figure 8. - Comparison of experimental and predicted heat transfer in $45^0$-$15^0$ nozzle operating with cooled inlet. Stagnation temperature $T_0$ = 811.1 K; stagnation pressure $P_0$ = 172.2 N/cm$^2$; throat diameter $D^*$ = 4.064 centimeters. Deficiency thicknesses at nozzle entrance: energy thickness $\varphi$ = 0.351 centimeter; momentum thickness $\theta$ = 0.264 centimeter; displacement thickness $\delta^*$ = 0.107 centimeter.